The Journal of Immunology

IL-10 Critically Modulates B Cell Responsiveness in *Rankl*$^{-/-}$ Mice

Veronica Marrella, Nadia Lo Iacono, Elena Fontana, Cristina Sobacchi, Heiko Sic, Francesca Schena, Lucia Sereni, Maria Carmina Castiello, Pietro Luigi Poliani, Paolo Vezzoni, Barbara Cassani, Elisabetta Traggiai and Anna Villa

J Immunol 2015; 194:4144-4153; Prepublished online 30 March 2015;
doi: 10.4049/jimmunol.1401977
http://www.jimmunol.org/content/194/9/4144

The Journal of Immunology is published twice each month by
The American Association of Immunologists, Inc.,
1451 Rockville Pike, Suite 650, Rockville, MD 20852

Print ISSN: 0022-1767 Online ISSN: 1550-6606.

IL-10 Critically Modulates B Cell Responsiveness in *Rankl*$^{-/-}$ Mice

Veronica Marrella,*,† Nadia Lo Iacono,*,† Elena Fontana,‡ Cristina Sobacchi,*,† Heiko Sic,§ Francesca Schena,¶ Lucia Sereni,‖ Maria Carmina Castiello,‖ Pietro Luigi Poliani,‡ Paolo Vezzoni,*,† Barbara Cassani,*,† Elisabetta Traggiai,§ and Anna Villa*,†

The immune and the skeletal system are tightly interconnected, and B lymphocytes are uniquely endowed with osteo-interactive properties. In this context, receptor activator of NF-κB (RANK) ligand (RANKL) plays a pivotal role in lymphoid tissue formation and bone homeostasis. Although murine models lacking RANK or RANKL show defects in B cell number, the role of the RANKL–RANK axis on B physiology is still a matter of debate. In this study, we have characterized in detail B cell compartment in *Rankl*$^{-/-}$ mice, finding a relative expansion of marginal zone B cells, B1 cells, and plasma cells associated with increased Ig serum levels, spontaneous germinal center formation, and hyperresponse to CD40 triggering. Such abnormalities were associated with an increased frequency of regulatory B cells and augmented B cell–derived IL-10 production. Remarkably, in vivo IL-10-R blockade reduced T cell–triggered plasma cell differentiation and restrained the expansion of regulatory B cells. These data point to a novel role of the RANKL–RANK axis in the regulation of B cell homeostasis and highlight an unexpected link between IL-10 CD40 signaling and the RANKL pathway. ***The Journal of Immunology*****, 2015, 194: 4144–4153.**

The receptor activator of NF-κB (RANK) ligand (RANKL) and its TNF-family receptor RANK are key players in bone homeostasis through the regulation of osteoclastogenesis and immune response (1–4). The RANK–RANKL axis shares the control of both molecular and cellular processes relevant for secondary lymphoid organ formation with lymphotoxin and TNF (5, 6). In vivo RANKL blockade selectively and transiently depletes thymus *Aire* and tissue-restricted Ag expression, thus creating a window of defective negative selection (7). The administration of soluble RANKL in a *Rankl*$^{-/-}$ mouse model dramatically improves bone and hematopoietic defects (8), further providing the in vivo evidence of the unique role played by RANKL in linking bone homeostasis to the immune system (9–11). It is largely accepted that B cells have a close and multifaceted relationship with bone cells (12). *Rank*$^{-/-}$ and *Rankl*$^{-/-}$ mice show a reduced peripheral B cell number associated with a lack of lymph nodes (1, 3, 13); however, B cell lymphopenia could reflect the dramatic reduction of B cell niche caused by the fibrosis of bone marrow (BM) cavity due to severe osteopetrosis. Despite the low B cell number, the role of RANK and RANKL in B cell physiology remains controversial. The reduction in B cell precursors and the block in the pro-B to pre-B cell progression in chimeric mice obtained by the transplant of *Rankl*$^{-/-}$ fetal liver cells into *Rag1*$^{-/-}$ recipient mice indicated a key role of RANKL in the development of B cell precursors (3). Consistently, specific deletion of *Rankl* in B cells confirmed its role in B cell development; however, to date a detailed characterization of the peripheral mature B cell phenotype and function has not been provided (14). On the contrary, the B cell–specific conditional knockout mouse for RANK showed no alteration in B cell development and function, suggesting that the RANK–RANKL axis is not directly involved in B cell physiology (15).

In humans, in the synovial joint fluid rheumatoid arthritis (RA), a subset of memory B cells produces high levels of RANKL, which stimulate osteoclastogenesis and bone resorption (16, 17). Our group showed defective Ig production and decreased frequency in the switched memory B cell population in osteopetrotic patients carrying mutations in the *RANK* gene (18). However, no gross B cell alteration was observed in autosomal recessive osteopetrosis due to a defect in the *RANKL* gene (19) (V. Marrella and A.Villa, unpublished data).

In this study, we report that in the complete absence of RANKL, mice show not only perturbation in the peripheral B cell distribution, but also in their functional properties. A significant expansion of marginal zone (MZ) B cells, splenic germinal centers (GC), B1, and plasma cells (PCs) associated with increased serum Ig levels was seen. The in vivo aberrant expansion of splenic GCs that rapidly shrink upon T-dependent challenge was well correlated with the in vitro hyperresponse to CD40 stimulation. Surprisingly, *Rankl*$^{-/-}$ mice do not show overt signs of autoimmunity or increased serum autoantibodies, and *Rankl*$^{-/-}$ B cells produce

*Istituto di Ricerca Genetica e Biomedica, Unità Operativa di Milano, Consiglio Nazionale delle Richerche, 20138 Milan, Italy; †Humanitas Clinical and Research Center, 20089 Rozzano, Italy; ‡Department of Molecular and Translational Medicine, Pathology Unit, University of Brescia, 25121 Brescia, Italy; §Novartis Institute for Research in Biomedicine, 4002 Basel, Switzerland; ¶Department of Pediatrics, University of Genova and Pediatrics II, Institute Giannina Gaslini, 16148 Genova, Italy; and ‖San Raffaele Telethon Institute for Gene Therapy, 20132 Milan, Italy

Received for publication August 4, 2014. Accepted for publication February 23, 2015.

This work was partially supported by Telethon Foundation Grant GGP12178 (to C.S.), European Community FP72012/SYBIL Grant 602300 (to A.V.), Progetti di Rilevante Interesse Nazionale Project Grant RF-2009-1499542 (to A.V.), and the Programma Nazionale per la Ricerca-Consiglio Nazionale delle Ricerche Aging Program 2012-2014 (to A.V. and P.V.).

Address correspondence and reprint requests to Dr. Anna Villa, Humanitas Clinical and Research Center, Via Manzoni 113, 20089 Rozzano, Italy. E-mail address: anna.villa@humanitasresearch.it

The online version of this article contains supplemental material.

Abbreviations used in this article: BM, bone marrow; Breg, B regulatory; DAB, diaminobenzidine; GC, germinal center; IONO, ionomycin; MZ, marginal zone; o/n, overnight; OPG, osteoprotegerin; PC, plasma cell; PNA, peanut agglutinin; RA, rheumatoid arthritis; RANK, receptor activator of NF-κB; RANKL, RANK ligand; RT, room temperature; Tfh, T follicular helper; WT, wild-type.

www.jimmunol.org/cgi/doi/10.4049/jimmunol.1401977

high amount of the anti-inflammatory IL-10 cytokine at the steady state and in response to CD40 and TLRs agonist. In vivo inhibition of IL-10 signaling caused reduction in the frequencies of splenic GCs, PCs, and regulatory B cells. Overall, these findings add a new role of RANKL to immune regulation and B cell homeostasis.

Materials and Methods

Mice immunization and treatment

Rankl$^{+/-}$ mice, a gift of Y. Choi (University of Pennsylvania), were maintained and genotyped, as described (8, 13). A total of 10^8 fresh SRBCs was injected i.p. in 5-wk-old *Rank*$^{-/-}$ mice and age-matched wild type (WT). T cell–independent Ag response was induced by i.p. injection of 115 μg Pneumovax-23 (Merck) in 5-wk-old mice (WT and *Rankl*$^{-/-}$). Anti–IL-10R (CD210; BD Pharmingen) mAb treatment was performed in mice at 5 wk of age. A total of 1 mg/20 mg mouse weight was administered i.p. in three separate doses at 3-d intervals. The mice were followed for 2 wk. Control mice were injected with IgG1 isotype Ab. All procedures involving animals were performed according to protocols approved by the Institutional Animal Care and Use Committee.

Flow cytometry and intracellular staining for IL-10

WT and *Rankl*$^{-/-}$ splenocytes, BM cells, and cells from coelomic cavities were prepared in FACS buffer (PBS supplemented with 0.5% BSA and 5 mM EDTA) and stained with the following specific fluorescent-conjugated Abs: B220, CD19, IgM, IgD, CD21, CD23, Fas, peanut agglutinin (PNA), CD4, CXCR5, ICOS, PD1, CD138, MHCII, CD69, and CD86. For IL-10 detection, 0.5×10^6 isolated CD19$^+$ cells were plated overnight (o/n) in medium alone or supplemented with LPS (1 μg/ml; R&D Systems) or CD40 (1 μg/ml; eBioscience, San Diego, CA). The day after, PMA (50 ng/ml; Sigma-Aldrich), ionomycin (IONO) (500 ng/ml; Sigma-Aldrich), and monensin (1 μg/ml; eBioscience) were added for the final 5 h; after surface staining, cells were fixed, permeabilized, and stained with IL-10 Ab (clone JES5-16ER; eBioscience), according to the manufacturer's instructions. All samples were acquired on a BD FACSCanto II flow cytometer (BD Biosciences, Franklin Lakes, NJ) and analyzed with FlowJo software (version 7.6.5; Tree Star, Ashland, OR). Abs were purchased from either BD Biosciences or eBioscience.

Histological analysis of splenic tissue

After sacrifice, tissue samples were formalin fixed and paraffin embedded or snap frozen in isopentane precooled in liquid nitrogen. Paraffin sections (2 μm) were used for routine H&E staining. The 5-μm–thick cryostat sections were air dried o/n at room temperature (RT) and fixed in acetone for 5 min before immunostaining with anti-mouse CD138 (clone 281-2 BD, 1:200), anti-MARCO (clone ED31, IgG1; AbD Serotec, Dusseldorf, Germany; 1:50), double staining with PNA (biotinylated anti-mouse B-1075; Vector Laboratories; 1:100), and IgD (FITC anti-mouse, 1:200) or double staining with MOMA-1 (rat anti-mouse monoclonal; Cedarlane Laboratories; 1:100) and CD1d (rat anti-mouse monoclonal; BD Biosciences; 1:1200). In brief, after peroxidase block (5 min) and rodent block (30 min), incubation with anti-CD138 was performed in da Vinci Green diluent (1 h) and in Rat-on-Mouse HRP-Polymer 15 min with final diaminobenzidine (DAB) development and counterstaining with H&E. Double staining with a mix of IgD and PNA primary Abs was carried out in da Vinci Green diluent (Biocare Medical) and secondary incubation with rat polymer alkaline phosphatase plus HRP-streptavidin. Staining was revealed with DAB and Ferangi Blue (Biocare Medical), and counterstaining was performed with Nuclear Fast Red (Sigma-Aldrich). Tissue sections for MZ B cells staining were prepared with anti–MOMA-1 (1 h at RT) and anti-CD1d (o/n at 4°C) primary Abs, incubated for 30 min with the appropriate secondary rat Ab (rat on mouse HRP or AP polymer kit; Biocare Medical), developed by both DAB and Ferangi Blue, and counterstained with methyl green. For staining with MARCO, tissue sections were incubated with primary rat anti-MARCO Ab o/n at 4°C and then for 30 min with anti-rat secondary Ab (Vector Laboratories; 1:200). The signal was revealed by ChemMATE Envision Rabbit/Mouse HRP/streptavidin-conjugated HRP (DAKO), followed by DAB and H&E as counterstain. For BrdU analysis, mice were i.p. injected with 1 mg BrdU solution (10 mg/ml in 1 × PBS) 1 h before sacrifice; the immunostaining with anti-mouse BrdU Ab (Serotec; 1:600) was performed following the manufacturer's instructions on splenic paraffin sections.

ELISA and ELISPOT

Levels of IgG isotypes, IgA, and IgM were measured in culture supernatants and sera by multiplex assay kit (Beadlyte Mouse Ig Isotyping kit; Millipore), according to the manufacturer's instructions, and run using a Bio-Plex reader (Bio-Rad Laboratories). IgE levels were determined by ELISA (BD Biosciences). IL-10 and osteoprotegerin (OPG) levels in supernatants and sera were measured with specific murine ELISA kits (R&D Systems). Ig-secreting cells were analyzed by ELISPOT using the species-specific purified and biotinylated anti-IgG and anti-IgM (Southern Biotech) and the 3-amino-9-ethylcarbazole (Sigma-Aldrich) as a chromogenic substrate.

RNA extraction and real-time quantitative PCR

RNA from splenic CD19$^+$ cells was extracted with TriZOL reagent following the suggested protocol (Invitrogen, Carlsbad, CA) and was reverse transcribed using the High Capacity cDNA Archive Kit, according to the manufacturer's instructions (Applied Biosystems). Expression of selected genes was quantified by Real Time-PCR from 50 ng cDNA in the presence of the SYBR Green PCR Master Mix (Applied Biosystems) using the DNA Engine Opticon 2 System (MJ Research). The primers used were the following: Actin, 5′-ctaaggccaaccgtgaaaag-3′ and 5′-accagaggcatacagggaca-3′; Blimp1, 5′-tgcggagaggctccacta-3′ and 5′-tgggttgctttccgtttg-3′; Bcl6, 5′-ttccgctacaagggcaac-3′ and 5′-cagcgatagggtttctcacc-3′; activation-induced cytidine deaminase, 5′-tcctgctcactggacttcg-3′ and 5′-gcgtaggaacaacaattccac-3′; Xbp1, 5′-tgacgaggttccagaggtg-3′ and 5′-tgcagaggtgcacatagtctg-3′; CD40, 5′-aaggaacgagtcagactaatgtca-3′ and 5′-agaaacaccccgaaaatggt-3′; CD40L, 5′-acgttgtaagcgaagccaac-3′ and 5′-tatcctttcttggcccactg-3′; $S1P_1$, 5′-gtgtagaccc-agagtcctgcg-3′ and 5′-agcttttccttggctggctggagag-3′; and $S1P_3$, 5′-ggagcccct-agacgggagt-3′ and 5′-ccgactgcgggaagagtgt-3′.

Determination of auto-Ab profile

Anti-IgG or anti-IgM dsDNA Abs were evaluated by ELISA. In brief, polystyrene plates were coated with poly-L-lysine (Sigma-Aldrich) and DNA from calf thymus (Sigma-Aldrich); after coating with 50 μg/ml polyglutamic acid for 45 min and blocking with PBS 3% BSA, serial dilutions of serum from 1:20 to 1:1280 were incubated o/n. Bound Ab was detected with alkaline phosphatase–conjugated goat anti-mouse IgG or IgM (Southern Biotech). The score of positivity was assigned to sera that were positive for dilution of 1:80 or higher.

Functional in vitro assays

CD19$^+$ cells were selected with magnetic microbeads, according to the manufacturer's instructions (Miltenyi Biotec), and were labeled with 0.5 μM CFSE (Invitrogen) for 8 min at RT. Labeled cells (30×10^4 cells) were cultured in a 96-well U-bottom plate with the following stimuli: 2.5 μg/ml IgM (Jackson ImmunoResearch Laboratories), 2.5 μg/ml CpG-B oligodeoxynucleotide (5′-tccatgacgttcctgacgtt-3′; Alexis), 10 μg/ml LPS (R&D Systems), or 1 μg/ml anti-CD40 (eBioscience). At day 5, the proliferation profile of viable CD19$^+$ cells, Ig, and IL-10 production in supernatants was analyzed.

Statistical analysis

Groups were analyzed with Prism Software (GraphPad) using a two-tailed Mann–Whitney unpaired test. Data are presented as mean ± SD. The p values <0.05 were considered significant. The χ^2 test was used to evaluate the statistical significance of the difference in the frequency of dsDNA Abs between the two groups (*Rankl*$^{-/-}$ mice and WT).

Results

Altered composition of the peripheral B cell compartment in Rankl$^{-/-}$ *mice*

Rankl$^{-/-}$ mice have a reduced B cell number in the BM due to the severe fibrosis caused by the excessive bone growth (1, 3, 8) (Supplemental Fig. 1A). Extramedullary hematopoiesis occurs in the spleen, as demonstrated by the increased splenic volume and higher proliferation rate in the red pulp (Supplemental Fig. 1B). Despite the increased splenic size, we observed a severe reduction in peripheral B cell compartment. Specifically, the frequency and the absolute number of total B cells (B220$^+$CD19$^+$) were significantly lower than in the WT counterpart with equal distribution among mature (M) and conventional transitional (T1, T2) subsets (Fig. 1A). The analysis of follicular (B220$^+$CD23^{high}CD21^{low}) and MZ B cells (B220$^+$CD23^{low}CD21^{high}) showed a significant relative increase of mature MZ B cell frequency, whereas no changes were observed in follicular compartment (Fig. 1B, *top panel*). The

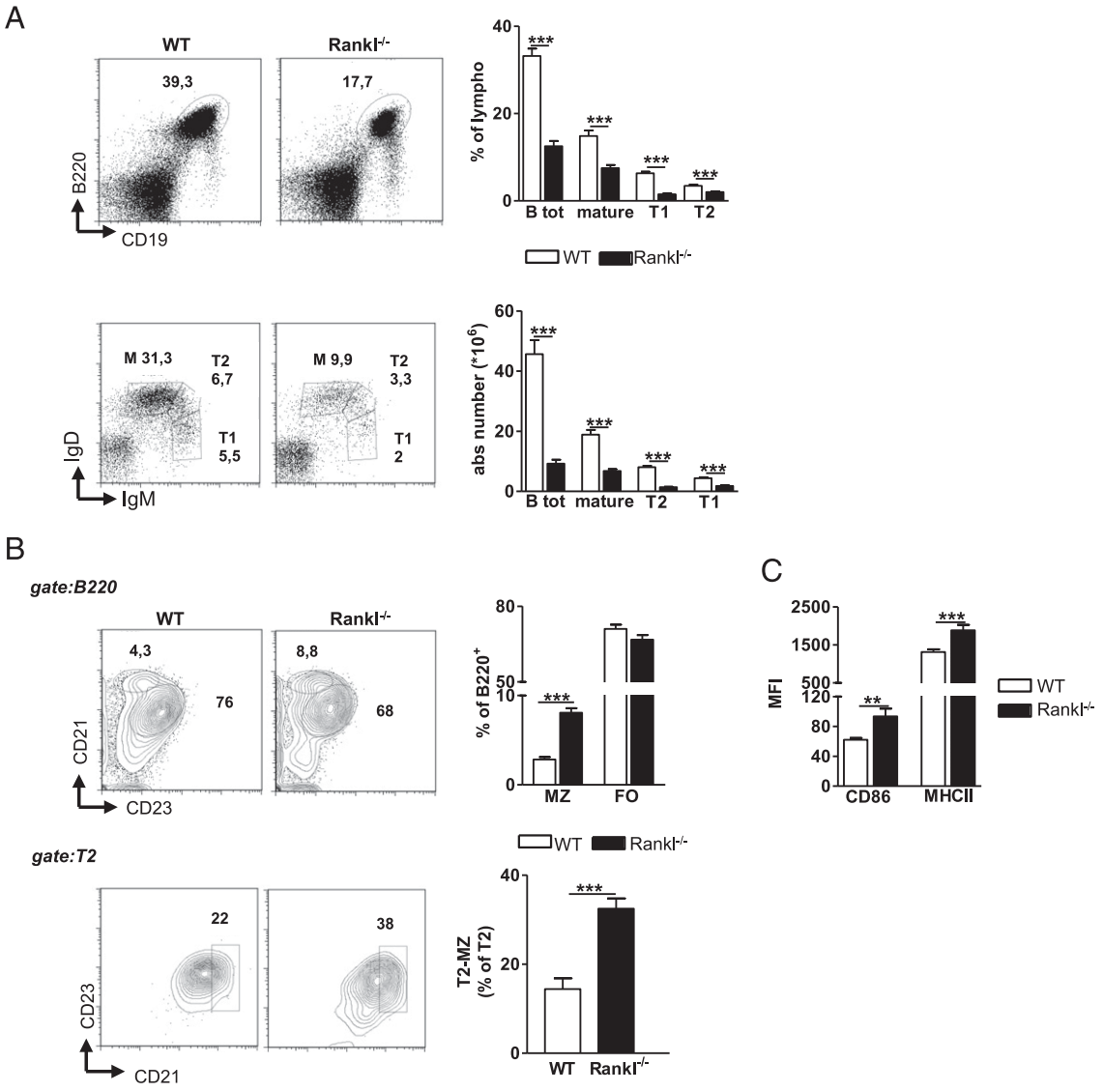

FIGURE 1. Reduced peripheral B cell compartment and expansion of MZ B cells in *Rankl*$^{-/-}$ mice. (**A**) *Left top and bottom*, Representative dot plot of splenic B220^{+}CD19^{+}, mature (M, IgM^{low}, IgD^{+}), transitional 1 (T1, IgM^{high}IgD^{-}), and transitional 2 (T2, IgM^{high}IgD^{+}) cells in WT and *Rankl*$^{-/-}$ mice. *Right top and bottom*, Graphic representation of the frequencies and the relative absolute number of all populations indicated in WT (n = 25) and *Rankl*$^{-/-}$ (n = 35) mice. (**B**) *Top and bottom left*, Dot plot of MZ and FO cells (gated on B220^{+}) and T2-MZ (gated on T2) in WT and *Rankl*$^{-/-}$ mouse. *Top and bottom right*, Graphic representation of FACS frequencies of these populations in all mice analyzed (WT n = 25, *Rankl*$^{-/-}$ n = 35). *Bottom left*, dot plot of T2-MZ cells in WT and *Rankl*$^{-/-}$ mouse. (**C**) Mean fluorescence intensity (MFI) for CD86 and MHCII on gated B220^{+}IgM^{+} cells in all mice analyzed (CD86 WT n = 10, *Rankl*$^{-/-}$ n = 11; MHCII WT n = 22, *Rankl*$^{-/-}$ n = 25). Numbers in the dot plots indicate the percentage of cells for each gate. Mean values ± SD are shown. $^{**}p < 0.01$, $^{***}p < 0.001$, Mann–Whitney test.

expansion of mature MZ B cells was sustained by the significant increase in the pool of MZ precursors (T2-MZ) identified in the gate of T2 cells on the basis of the high expression of CD21 (Fig. 1B, *bottom panel*). Notably, *Rankl*$^{-/-}$ IgM^{+} B cells evaluated for the expression of CD86 and MHCII activation markers showed a higher mean fluorescence intensity when compared with WT littermates (Fig. 1C).

Aberrant localization of Rankl$^{-/-}$ *MZ B cells and downregulation of S1P receptors in Rankl*$^{-/-}$ *B cells*

We stained splenic sections with Abs against metallophilic macrophages (MOMA-1), localized at the border between the marginal and the follicular area, and MZ B cells (CD1d). Immunohistochemical analysis confirmed the expansion of MZ B cells and showed an altered distribution of CD1d^{+} cells in mutant spleens. Moreover, *Rankl*$^{-/-}$ CD1d^{+} cells were randomly distributed both in and outside and inside the border defined by MOMA-1 when compared with WT spleen, where MZ B cells were mainly located externally to the ring composed of MOMA-1^{+} cells (Fig. 2A [*top panels*], 2B) Furthermore, *Rankl*$^{-/-}$ MOMA-1^{+} cells were distributed around the follicle, forming a discontinuous ring (Fig. 2A), thus confirming data previously described (3). To further investigate the defective localization of CD1d^{+} cells, we stained splenic sections with anti-MARCO mAb recognizing a distinct population of MZ macrophages involved in the retention of B cells in the MZ (20). As shown in Fig. 2A (*lower panels*), we did not detect any relevant difference in MARCO^{+} cell distribution. Because S1P is a factor involved in MZ B cell positioning and shuttling to the follicle (21), we tested the expression of $S1P_1$ and $S1P_3$ receptors on B cells. We observed that both receptors were significantly downregulated on *Rankl*$^{-/-}$ B cells (Fig. 2C), according to the MZ B cell displacement described above.

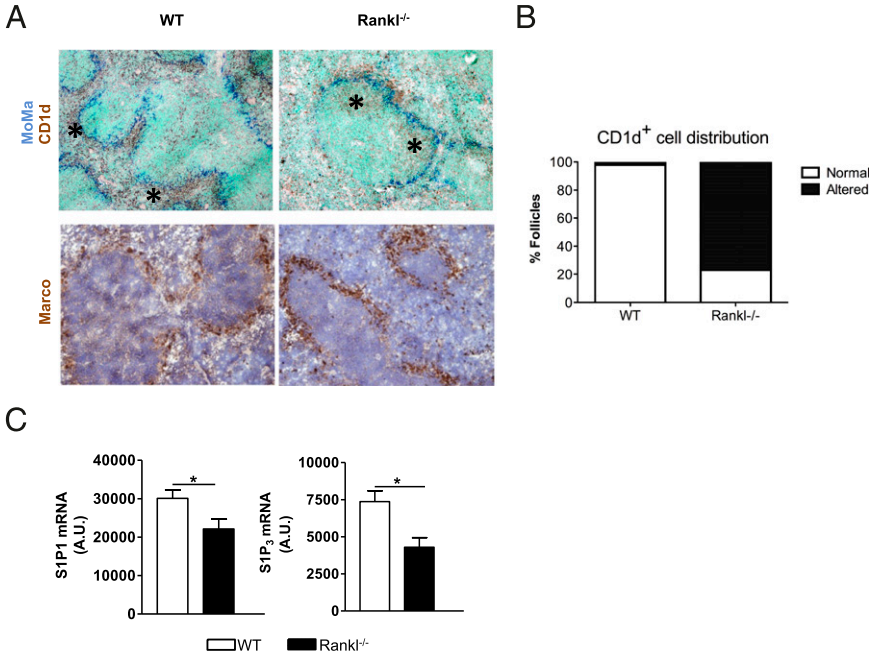

FIGURE 2. Aberrant localization of MZ *Rankl*$^{-/-}$ B cells in the splenic MZ. (**A**) *Top*, Double immunostaining for MZ B cells (CD1d, brown) and metallophillic macrophages (MOMA-1, blue). Original magnification ×10. Asterisks indicate the localization of CD1d MZ B cells across (*Rankl*$^{-/-}$) and outside (WT) the MOMA ring. *Bottom*, Immunostaining for splenic MZ macrophages (MARCO, brown) in a representative WT and *Rankl*$^{-/-}$ mouse. Original magnification ×10. (**B**) Relative proportion of follicles with normal and altered distribution of CD1d^{+} cells around the MOMA ring. Mean values are shown from WT (n = 4) and *Rankl*$^{-/-}$ mice (n = 4), in which $n \geq 10$ follicles have been analyzed by a blinded investigator. (**C**) Real-time analysis for $S1P_1$ and $S1P_3$ receptors on purified splenic CD19^{+} cells from WT (n = 6) and *Rankl*$^{-/-}$ mice (n = 5). Mean values ± SD are shown. *$p < 0.05$, Mann–Whitney test.

Expansion of B1 cells contributes to high serum IgM levels in Rankl$^{-/-}$ *mice that normally respond to T-independent Ags*

Despite peripheral B cell lymphopenia, *Rankl*$^{-/-}$ mice presented significantly increased levels of serum IgM (Fig. 3A). To evaluate whether B1 cells could contribute to the increased production of IgM Abs in the serum as MZ B cells do (22), we analyzed the B1 B cell subset in the coelomic cavities (peritoneum and pleura). A significant expansion in the frequency and absolute number of B1 B cells (CD23^{+}IgM^{-}) was found in *Rankl*$^{-/-}$ mice compared with WT (Fig. 3B). This finding was consistent with the increased frequency of B1a B cell fraction (CD23^{low}IgM^{+}CD5^{high}), a population of precursor B1 cells in the coelomic cavities (23) and in the spleen of mutant mice (Fig. 3C). Because B1 and MZ B cells are mainly responsible for T-independent Ab response in humoral defenses (24), we investigated whether *Rankl*$^{-/-}$ mice were able to properly respond to a polysaccharide vaccine. To this end, 5-wk-old *Rankl*$^{-/-}$ and WT mice were challenged i.p. with a vaccine containing a mixture of T-independent polysaccharide Ags (Pneumovax23-P23), and the

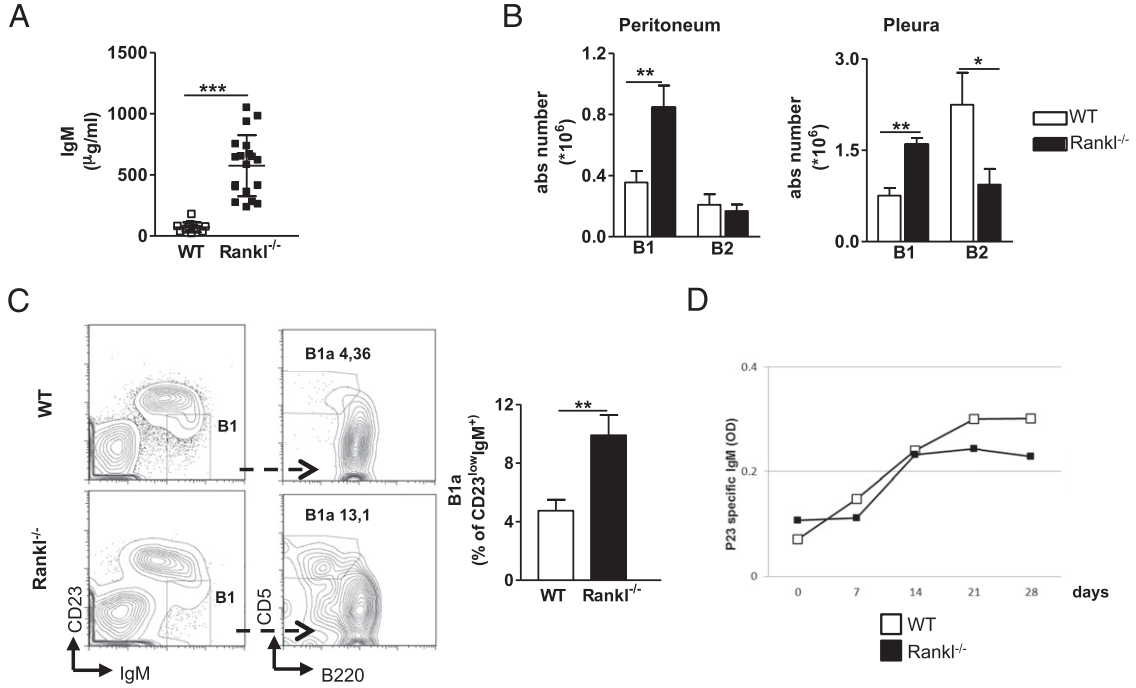

FIGURE 3. Expansion of B1 cells contributes to the increased serum IgM level in *Rankl*$^{-/-}$ mice that show an intact response to T-independent Ags. (**A**) IgM serum level in WT (n = 12) and *Rankl*$^{-/-}$ mice (n = 19). (**B**) Absolute number of B1 and B2 cells in the peritoneum (WT n = 11, *Rankl*$^{-/-}$ n = 15) and in the pleura (WT n = 5, *Rankl*$^{-/-}$ n = 7). (**C**) *Left*, Dot plot for B1 population (CD23^{low}IgM^{+}) in which B1a cells (B220^{-}CD5^{+}) are gated in a representative WT and *Rankl*$^{-/-}$ mouse; numbers indicate the percentage of cells for each gate. *Right*, Frequencies of splenic B1a cells in all mice analyzed (WT n = 16, *Rankl*$^{-/-}$ n = 23). (**D**) Anti-P23–specific IgM Ab titers at different days after challenge. Mean values ± SD are shown. *$p < 0.05$, **$p < 0.01$, ***$p < 0.001$, Mann–Whitney test.

production of specific Abs was quantified in the sera every week after the challenge until 1 mo when the animals were sacrificed. *Rankl*$^{-/-}$ mice showed normal production of P23-specific IgM Abs, suggesting no defect in specific humoral immune response (Fig. 3D).

Expansion of aberrantly localized PCs expressing higher MHCII in Rankl$^{-/-}$ *mice is confirmed by a skewed transcriptional program in Rankl*$^{-/-}$ *B cells*

Both MZ and B1 B cells can rapidly differentiate into short-lived PCs independently, without T cell help (25). In agreement with the expansion of these two populations, we detected a higher frequency of B220$^{-/low}$CD138^{+} cells in the spleen of mutant mice, which express a significantly higher level of MHCII than WT controls (Fig. 4A). ELISPOT analysis performed on *Rankl*$^{-/-}$ splenocytes further confirmed the significant increase in IgM- and IgG-secreting cells (Fig. 4B). In accordance with the expansion of IgG-secreting cells, significantly increased levels of serum IgG2a, IgG2b, and IgG3 were observed (Fig. 4C), a tendency to increased IgG1 levels, whereas IgA and IgE levels were comparable to WT (Supplemental Fig. 2). To better characterize PC distribution, we stained splenic sections with CD138 surface marker. In *Rankl*$^{-/-}$ mice, CD138^{+} cells localized ectopically in the spleen, and were mainly distributed outside the white pulp area and not in the red pulp, as normally occurs in WT mice (Fig. 4D). Next, we investigated the molecular program sustaining PC differentiation. We found a significant increased expression of Blimp1 in splenic *Rankl*$^{-/-}$ CD19^{+} cells, accompanied by higher Xbp1 and decreased Bcl6 expression. Consistently with higher levels of switched Ig, higher expression of the activation-induced cytidine deaminase gene transcript was detected (Fig. 4E).

Rankl$^{-/-}$ *mice present aberrant number and size of GCs in the spleens, in vitro B cell hyperresponsiveness to CD40 triggering, but defective T cell–dependent response*

To address whether the expansion of IgG PC compartment could derive from GC reactions, we evaluated the expression of PNA and Fas, surface markers defining GC B cells. We found a statistically increased frequency of PNA^{+}Fas^{+} CD19^{+} cells in *Rankl*$^{-/-}$ mice (Fig. 5A, *top panel*). We further confirmed these findings by immunohistochemical analysis of spleen sections with PNA (brown) and IgD (blue) Abs (Fig. 5A, *bottom left panel*) quantifying the number of GCs in the total area of each splenic section (Fig. 5A, *bottom right panel*). Accordingly, we found a significant increase in the frequency of T follicular helper (Tfh) cells (ICOS^{+}PD1^{+}) (Supplemental Fig. 3), a T cell subset involved in GC maintenance (26). The relevant expansion of MZ B, B1 cells, PCs, and GCs is usually associated with increased susceptibility to develop autoimmunity (27–29). Interestingly, we did not detect a significant increase in the percentage of *Rankl*$^{-/-}$ mice positive for anti-dsDNA Abs in the sera. Next, we tested the in vitro proliferative response of *Rankl*$^{-/-}$ CD19^{+} cells to different stimuli, including BCR, TLRs, and CD40. Interestingly, *Rankl*$^{-/-}$ CD19^{+} B cells showed significantly increased proliferative activity compared with WT B cells only upon CD40 triggering (Fig. 5B, *left panel*). Moreover, in response to CD40, significant higher amounts of all Ig subtypes were found in the supernatant of *Rankl*$^{-/-}$ CD19^{+} B cells (Fig. 5B, *right panel*). Of note, despite the fact that no differences in proliferative response to other stimuli were present, we detected an overproduction of Ig at the steady state and upon BCR and TLR stimulation (data not shown). It is known that mature B cells produce OPG cytokine in response to CD40 (30).

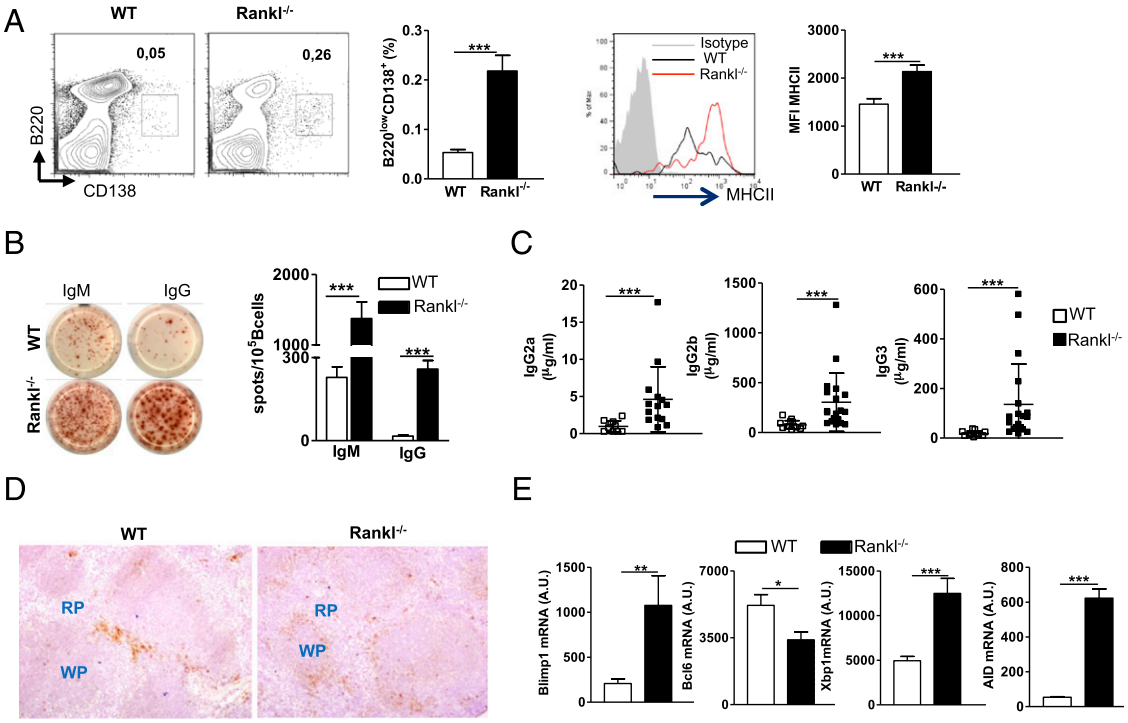

FIGURE 4. PC compartment is expanded in *Rankl*$^{-/-}$ mice. (**A**) *Left*, Dot plot representing PCs in WT and *Rankl*$^{-/-}$ mouse and PC percentages in all mice analyzed (WT $n = 28$, *Rankl*$^{-/-}$ $n = 36$). *Right*, Expression of MHCII on gated B220^{low}CD138^{+} in WT (black line) and *Rankl*$^{-/-}$ (red line) mouse, isotype control is shown (gray line), and MHCII mean fluorescence intensity values in all mice analyzed (WT $n = 28$, *Rankl*$^{-/-}$ $n = 38$). (**B**) ELISPOT assay on total splenocytes for IgM and IgG in a representative WT and *Rankl*$^{-/-}$ mouse and number of spots obtained from 9–10 mice/group analyzed and normalized to 10^5 B220^{+} cells. (**C**) Level of IgG2a, IgG2b, and IgG3 measured in the sera from WT ($n = 12$) and *Rankl*$^{-/-}$ mice ($n = 19$). (**D**) Representative immunostaining for CD138 on frozen splenic sections from WT and *Rankl*$^{-/-}$ mouse. Original magnification ×10. Red pulp (RP) and white pulp (WP) are indicated. (**E**) Real-time analysis for B cell transcription factor expression on selected CD19^{+} cells from WT ($n = 9$) and *Rankl*$^{-/-}$ ($n = 9$) mice. Mean values ± SD are shown. *$p < 0.05$, **$p < 0.01$, ***$p < 0.001$, Mann–Whitney test.

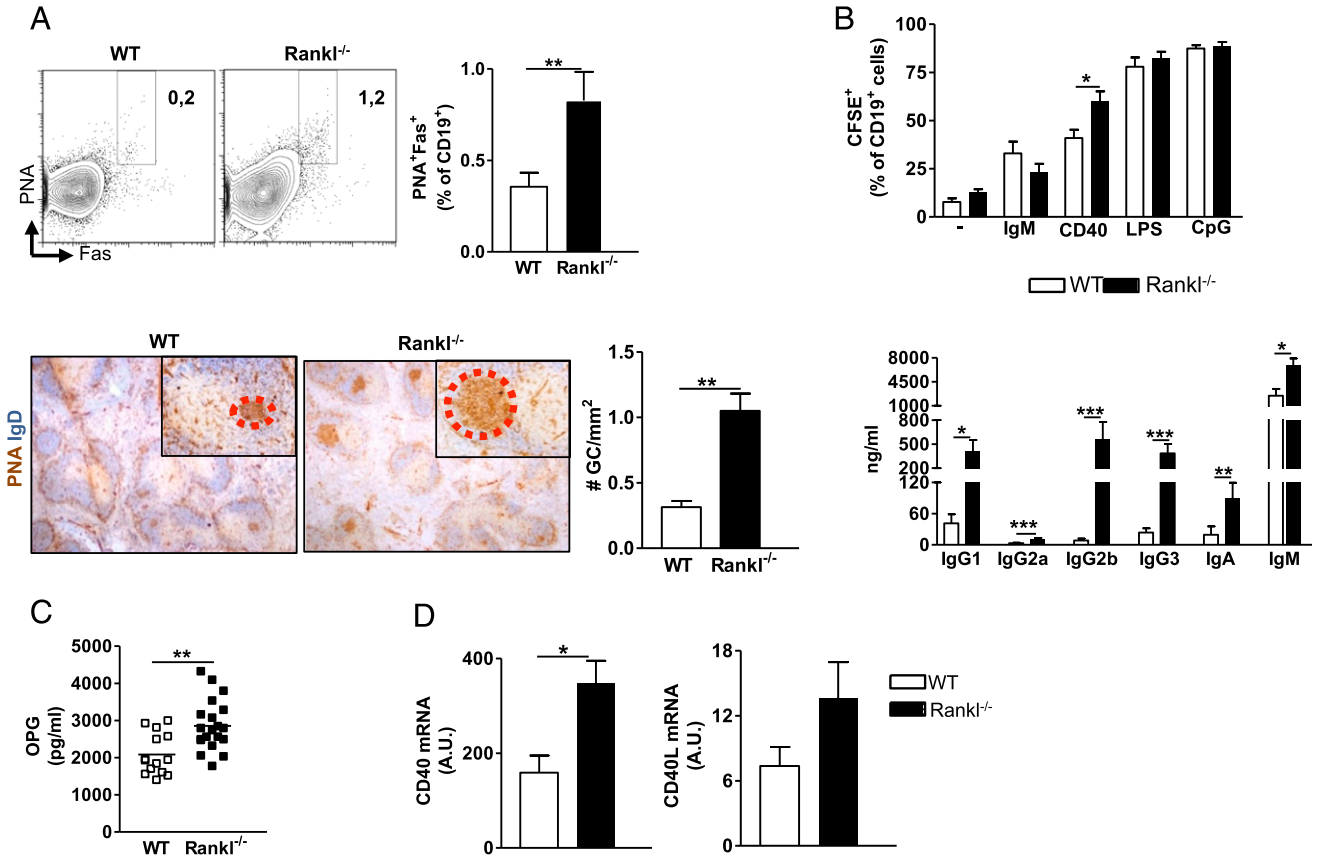

FIGURE 5. Hyperresponse of *Rankl*$^{-/-}$ B cells to CD40 signaling. (**A**) *Top*, Dot plot for identification of GCs in gated CD19^{+}B220^{+} cells stained with PNA and Fas Abs and FACS percentages of GCs in all mice analyzed (WT $n = 32$, *Rankl*$^{-/-}$ $n = 36$). *Bottom*, Representative immunostaining for GCs (PNA, blue; IgD, brown) in WT and *Rankl*$^{-/-}$ spleen. Original magnification ×4; the *insets* (original magnification ×10) highlight the different size of the GC in WT and *Rankl*$^{-/-}$ spleen. Histograms showing the number of GCs present in the spleen section of each mouse analyzed (WT $n = 6$, *Rankl*$^{-/-}$ $n = 6$). (**B**) *Left*, FACS percentages of CD19^{+}CFSE^{+} proliferating cells at day 5 in the conditions indicated for all mice analyzed (WT $n = 9$, *Rankl*$^{-/-}$ $n = 10$). *Right*, Concentrations of indicated Ig isotypes measured in supernatants in presence of CD40 stimulus. (**C**) OPG levels measured by ELISA in the sera of WT ($n = 12$) and *Rankl*$^{-/-}$ ($n = 19$) mice. (**D**) Real-time analysis for CD40 and CD40L in purified splenic CD19^{+} cells obtained from WT ($n = 6$) and *Rankl*$^{-/-}$ mice ($n = 6$). $*p < 0.05$, $**p < 0.01$, $***p < 0.001$, Mann–Whitney test.

Indeed, in the sera of *Rankl*$^{-/-}$ mice, we detected significant higher concentration of OPG than that compared with its WT counterpart (Fig. 5C). We also measured the expression of CD40 and CD40L on purified *Rankl*$^{-/-}$ B cells, finding significant up-regulation of the receptor, whereas the ligand transcript showed only a tendency to be higher (Fig. 5D). All together, these observations suggest that *Rankl*$^{-/-}$ B cells show hyperresponsiveness to CD40 signaling. Next, we tested the formation of GCs in response to T-dependent Ag immunization, challenging *Rankl*$^{-/-}$ and WT mice with SRBC. Twelve days after the challenge, GC formation in the spleen was analyzed. Surprisingly, whereas GCs in the WT mice increased in size, these structures in *Rankl*$^{-/-}$ mice diminished in volume (Fig. 6).

Rankl$^{-/-}$ *B cells show increased production of IL-10–promoting B cell activation*

Constitutively CD40-activated B cells are known to drive expansion of IL-10–producing B cells (31). Hence, we analyzed the production of IL-10 in purified B cells obtained from *Rankl*$^{-/-}$ and WT spleen after o/n stimulation with LPS or CD40 in combination with PMA/IONO for the last 5 h by intracellular staining. *Rankl*$^{-/-}$ mice showed a significant increased frequency of IL-10– producing B cells at the steady state and upon CD40 and LPS triggering (Fig. 7A). To evaluate whether the IL-10 production could be maintained over a long period, we measured this cytokine in supernatants of B cells cultured for 5 d in the presence of different stimuli. *Rankl*$^{-/-}$ B cells showed a significantly higher IL-10 concentration in each condition analyzed (Fig. 7B). IL-10– producing B cells play a regulatory role in autoimmune diseases by preventing or reducing autoimmune pathogenesis, restoring immune homeostasis, and repressing antitumor immune responses (32, 33). We stained CD19^{+} cells with CD1d and CD5, markers for a specific B regulatory (Breg) cell subset identified as the major subset responsible for the in vivo production of IL-10, the so-called B10 cells (34) and we found a significantly higher frequency of this population in *Rankl*$^{-/-}$ mice compared with the WT (Fig. 7C). To further understand whether the increased IL-10 expression could impact on B cell phenotype in the absence of RANKL, mutant mice were treated with an antagonist of IL-10R (CD210) and followed for 2 wk. After sacrifice, mice were analyzed for the presence of mature GC, frequency of PCs, and Breg cells. A significant decrease in the proportion of splenic PNA^{+} Fas^{+} GC B cells was observed upon the treatment in mutant animals (Fig. 8A). Accordingly, a consistent reduction in serum IgM and IgG levels was present in treated affected animals, which correlates with decreased CD138^{+} PCs (Fig. 8B, Supplemental Fig. 4). No change in the autoantibodies production was observed. To investigate the contribution of T cell help in the induction and maintenance of GC during the treatment, we evaluated the proportion of Tfh cells, and found a marked reduction of this population in

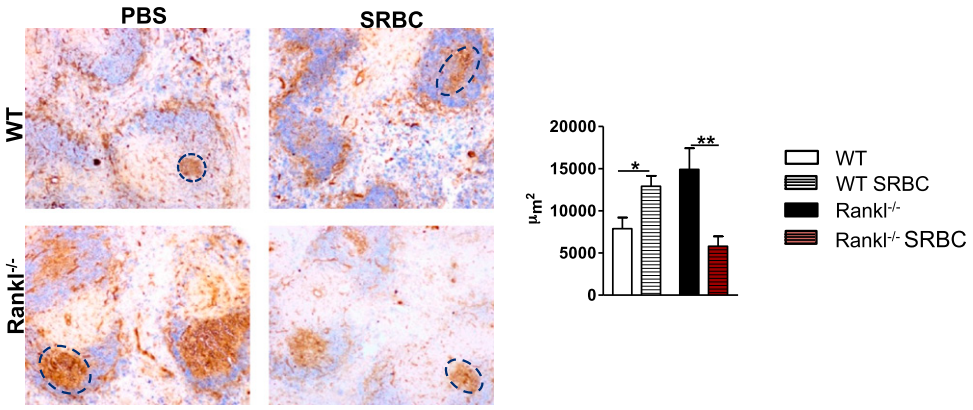

FIGURE 6. *Rankl*$^{-/-}$ mice show defective T cell–dependent response. *Left*, Splenic sections stained with PNA and IgD for a representative WT and *Rankl*$^{-/-}$ mouse for each group indicated. Dashed circles indicate the GC area. Original magnification ×10. *Right*, Area of GCs in the spleens of all mice/group analyzed (WT PBS $n = 6$, WT SRBC $n = 6$, *Rankl*$^{-/-}$ PBS $n = 7$, *Rankl*$^{-/-}$ SRBC $n = 6$). *$p < 0.05$, **$p < 0.01$, Mann–Whitney test.

the spleen of *Rankl*$^{-/-}$ treated mice (Fig. 8C), in the absence of alterations in the overall CD4$^+$ and CD8$^+$ T cell compartments. Furthermore, the proportion of Breg cells, both the CD1d$^+$CD5$^-$ and CD1d$^+$CD5$^+$ B cell subsets, was significantly affected by the in vivo blockade (Fig. 8D) and most likely reflects a contraction in the MZ B cells (Supplemental Fig. 4). Overall, these findings highlight a crucial role for IL-10 signaling in the immune dysregulation consequent to RANKL deficiency.

Discussion

RANKL is an important player in the close link between the immune compartment with the bone system (3, 9, 35). B cells are key actors in the adaptive and innate immunity because their early development is in close contact with skeletal system cells that produce factors for bone maintenance (12). The reciprocal interaction between B lymphocytes and the skeletal system is demonstrated by the fact that the deletion of transcription factors regulating B cell differentiation affects bone mass; vice versa, inactivation of bone cell functions results in B cell developmental block (36). *Rankl*$^{-/-}$ and *Rank*$^{-/-}$ mice present a dramatic reduction in B cell number both in BM and spleen; however, the role played by the RANKL–RANK axis in regulating B cell development and function is still unclear. We show in this study that RANKL deficiency is responsible for a perturbation in B cell distribution and homeostasis. Within the reduced peripheral B cell pool, an expansion of B cell subpopulations MZ B, B1 cells, and PCs was detected. Consistently, increased levels of Ig were found in the serum of *Rankl*$^{-/-}$ mice. The presence of aberrant GC formation frequently represents a sign of autoimmune condition (29). Of note, *Rankl*$^{-/-}$ mice showed more GCs with a higher size than those observed in WT. Despite these findings, we did not detect a significant increase of autoantibodies in the sera of young and adult *Rankl*$^{-/-}$ mice. Additionally, B cells lacking RANKL displayed an increased proliferative response and increased production of Ig upon CD40 triggering. Because CD40 signaling is known to be involved in GC formation and maintenance (37), the increased number of GCs in *Rankl*$^{-/-}$ mice suggested a hyperresponse of mutant B cells to CD40. Notably, upon T cell–dependent stimulus, GCs from *Rankl*$^{-/-}$ mice undergo a premature regression similar to models in which the magnitude of CD40 signaling was intensified (38–40).

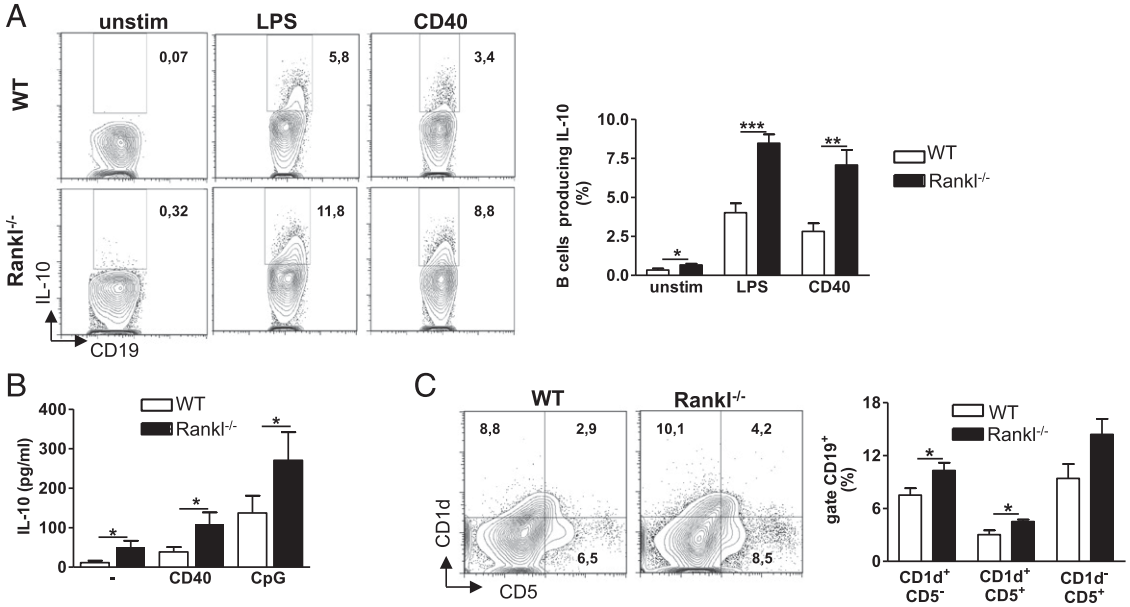

FIGURE 7. *Rankl*$^{-/-}$ B cells produce high amount of IL-10. (**A**) Dot plots of intracellular IL-10 production upon the indicated stimuli in purified CD19$^+$ cells for a representative WT and *Rankl*$^{-/-}$ mouse. Bars represent the FACS frequencies of B cells producing IL-10 in the experimental conditions indicated for all mice analyzed (WT $n = 10$, *Rankl*$^{-/-}$ $n = 10$). (**B**) IL-10 concentration at day 5 in the supernatants of cultured CD19$^+$ cells in the conditions indicated for all mice used in the experiments (WT $n = 9$, *Rankl*$^{-/-}$ $n = 9$). (**C**) *Left*, Dot plot for the identification of splenic CD1d$^+$CD5$^+$ Bregs of a representative WT and *Rankl*$^{-/-}$ mouse. Bars resume the FACS percentages for the populations indicated in WT ($n = 9$) and *Rankl*$^{-/-}$ ($n = 10$) mice. *$p < 0.05$, **$p < 0.01$, ***$p < 0.001$, Mann–Whitney test.

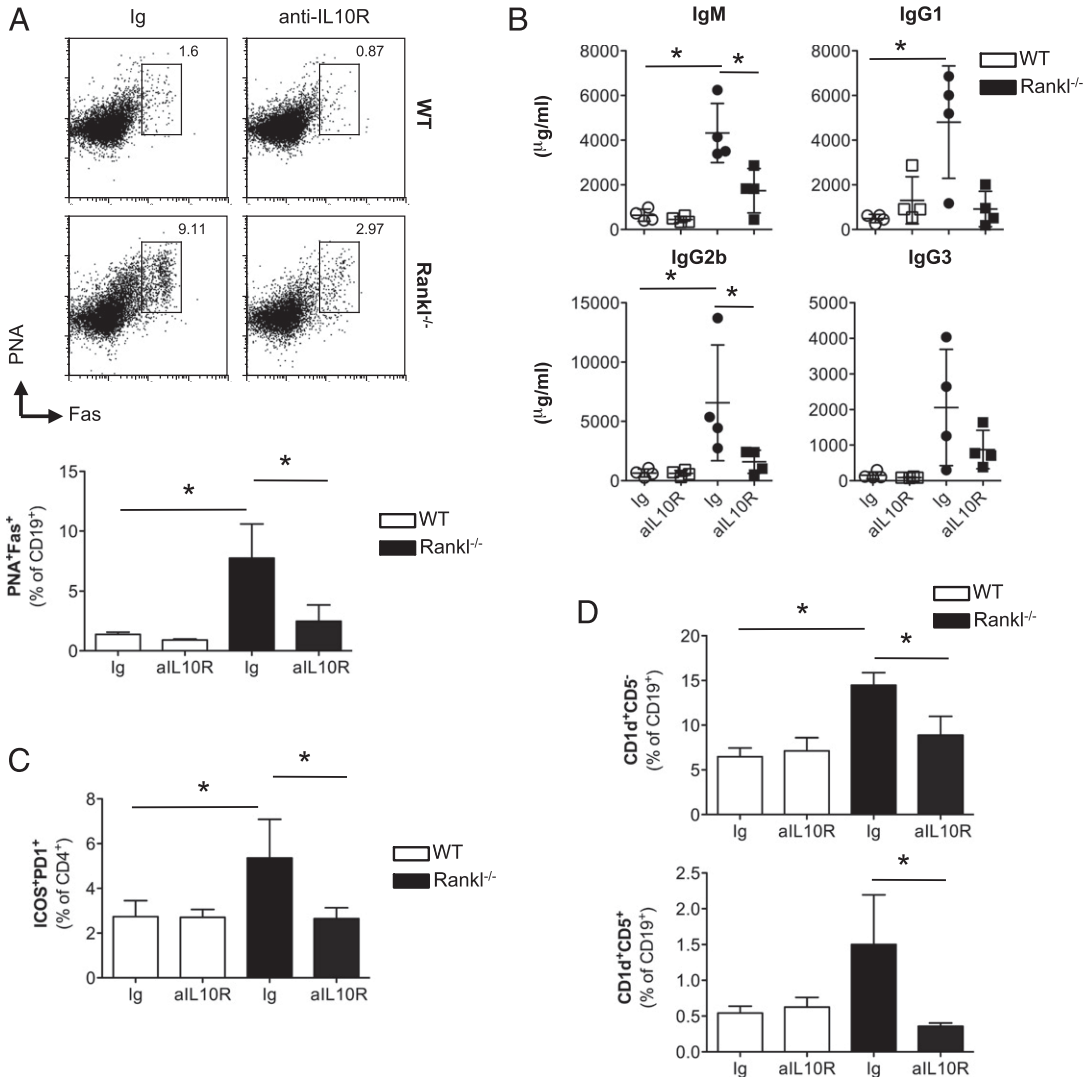

FIGURE 8. IL-10R signaling sustains B cell dysregulation in *Rankl*$^{-/-}$ mice. Mice were injected with anti–IL-10R mAb in three separate doses, starting at 5 wk of age and followed for 2 wk after the end of the treatment. After sacrifice, splenic cells were analyzed and sera were collected. (**A**) Representative dot plots showing the flow cytometric analysis of PNA^{+}Fas^{+} (GC) cells gated on total CD19^{+} B cells. The numbers in the dot plot quadrants represent the percentages. Bars of the graph represent the FACS frequencies of GC B cells in the experimental conditions indicated for all mice analyzed (WT $n = 4$, *Rankl*$^{-/-}$ $n = 4$/condition). Mean values ± SD are shown. Data are representative of two experiments. (**B**) Level of IgM, IgG1, IgG2b, and IgG3 measured in the sera from WT ($n = 4$) and *Rankl*$^{-/-}$ mice ($n = 4$) treated or not with the blocking Ab. (**C**) FACS frequencies of ICOS^{+}PD1^{+} cells gated on splenic CD4^{+} T cell subset. Each bar represents mean values ± SD from $n = 4$ mice/group. Data are representative of two experiments. (**D**) FACS percentages of CD1d^{+}CD5^{-} and CD1d^{+}CD5^{+} cells on total CD19^{+} B cells. Each bar represents mean values ± SD from $n = 4$ mice/group. Data are representative of two experiments. *$p < 0.05$, Mann–Whitney test.

The CD40L/CD40 pathway has functional similarities to RANKL/RANK, and previous evidences suggest that their interplay is crucial to ensure proper T cell responses in vivo (41). In this study, we provide evidence that RANKL/RANK and CD40L/CD40 systems cooperate also to influence T cell–dependent B cell responses.

OPG cytokine, the soluble decoy receptor of RANKL, is a potent inhibitor of osteoclastogenesis (42) and also regulates B cell development and function (43). More interestingly, OPG production by B cells in vivo is promoted through CD40 costimulation (30). Consistently with our hypothesis of hyperresponsiveness to CD40 triggering, we found high serum levels of OPG in *Rankl*$^{-/-}$ mice.

IL-10 is an anti-inflammatory cytokine with a crucial role in controlling inflammatory response, as demonstrated by the occurrence of several autoimmune diseases in IL-10 deficiency (44, 45). B cells with suppressive regulatory activity performed through IL-10 production have been described in various animal models and human conditions, as reviewed previously (34, 46). In mice T2-MZ B, MZ B, CD5^{+} B1, and CD1d^{+}CD5^{+} B cells have been described as producing IL-10 with regulatory effects (32). Notably, *Rankl*$^{-/-}$ mice have an increased frequency of these B cell subpopulations. Amplified CD40 signaling has been shown to drive B cells to produce IL-10 (31), and agonistic anti-CD40 Ab induces enrichment of IL-10–producing T2-MZ cells that once transplanted reverse autoimmunity in MLR/*lpr* mice (47). Consistently with these data, in *Rankl*$^{-/-}$ B cells we detected higher production of IL-10 by intracellular staining and in culture supernatants at the steady state and upon CD40 or TLR stimulation. Intriguingly, recent studies have identified plasmablasts/PCs as the main types of effector B cells producing cytokines such as IL-10, IL-35, TNF-α, IL-17, and GM-CSF (48). Accordingly, *Rankl*$^{-/-}$ mice showed an enlargement of PC population, which could also contribute to IL-10 secretion (49, 50). An expansion of B cell–derived IL-10 cells has also been reported in association

with suppression of Th1 inflammatory response (49). We also observed that *Rankl*$^{-/-}$ T cells once stimulated with PMA/IONO produce less IFN-γ than WT cells (data not shown). In *Rankl*$^{-/-}$ mice a perturbed B cell compartment, together with the recognized role of RANKL in the correct maintenance of central tolerance (51), could easily induce autoimmunity; nevertheless, mutant mice did not present significant levels of serum autoantibodies and did not show any signs of autoimmune pathology. Our results indicate that an amplified response to CD40L occurs in the absence of RANKL, leading to an increased IL-10 production by B cells, thus generating an anti-inflammatory environment that together with the absence of lymph nodes might prevent the development of overt autoimmune signs. To further address the contribution of augmented IL-10 production in dampening inflammatory response, we treated mutant mice and wild-type controls with an anti–IL-10R Ab. The in vivo blockade of IL-10 signaling resulted in a decreased proportion of Breg cells in the *Rankl*$^{-/-}$ mice, suggesting that autocrine IL-10 is critical for the maintenance of this IL-10–competent B cell subset. Despite Breg reduction, we could not detect any change in tissue organ infiltration and serum autoantibodies (data not shown) in the mutant mice. However, we cannot exclude the possibility that our results are affected by the short kinetics of the treatment, caused by the limited lifespan of mutant mice due to the bone defect. In contrast, we observed a significant reduction of splenic GC B cells associated with lower serum IgM and IgG levels. In agreement with these data, the Ab treatment markedly affected *Rankl*$^{-/-}$ Tfh cell subset, a compartment required for the formation of GC B cells and PC generation (52). IL-10 is known to induce activated B cell expansion and differentiation into Ab-producing cells that secrete a large amount of Ig Abs (53–55). Thus, our results suggest that IL-10 might impose this effect through the regulation of Tfh cells.

A population of memory B cells in the synovial fluid of RA patients has been reported to secrete RANKL and proinflammatory cytokines participating to bone erosion (16, 17), and levels of RANKL in the synovial fluid of RA patients are significantly reduced following treatment with rituximab (anti-CD20 mAb), suggesting a link between B cell inflammation and bone destruction (56). Currently, anti-human RANKL (Denosumab) administration is in phase II for the treatment of RA in which autoimmunity and inflammation contribute to increase bone erosion (57). Our findings demonstrate that the inhibition of RANKL not only acts on bone resorption, but also modulates the inflammatory environment by increasing B cell responsiveness to CD40L and the level of IL-10 production, which unexpectedly sustains B cell activation in a positive feedback loop. Thus, further investigations are needed to fully dissect the potential effect of Denosumab on the immune system.

Acknowledgments

We thank Prof. Yongwon Choi for providing *Rankl*$^{+/-}$ mice. The technical assistance of Stefano Mantero is acknowledged.

Disclosures

The authors have no financial conflicts of interest.

References

1. Dougall, W. C., M. Glaccum, K. Charrier, K. Rohrbach, K. Brasel, T. De Smedt, E. Daro, J. Smith, M. E. Tometsko, C. R. Maliszewski, et al. 1999. RANK is essential for osteoclast and lymph node development. *Genes Dev.* 13: 2412–2424.
2. Anderson, D. M., E. Maraskovsky, W. L. Billingsley, W. C. Dougall, M. E. Tometsko, E. R. Roux, M. C. Teepe, R. F. DuBose, D. Cosman, and L. Galibert. 1997. A homologue of the TNF receptor and its ligand enhance T-cell growth and dendritic-cell function. *Nature* 390: 175–179.
3. Kong, Y. Y., H. Yoshida, I. Sarosi, H. L. Tan, E. Timms, C. Capparelli, S. Morony, A. J. Oliveira-dos-Santos, G. Van, A. Itie, et al. 1999. OPGL is a key regulator of osteoclastogenesis, lymphocyte development and lymph-node organogenesis. *Nature* 397: 315–323.
4. Wang, R., L. Zhang, X. Zhang, J. Moreno, C. Celluzzi, M. Tondravi, and Y. Shi. 2002. Regulation of activation-induced receptor activator of NF-kappaB ligand (RANKL) expression in T cells. *Eur. J. Immunol.* 32: 1090–1098.
5. Fritz, J. H., and J. L. Gommerman. 2010. Cytokine/Stromal cell networks and lymphoid tissue environments. *J. Interferon Cytokine Res.* 31: 277–289.
6. Koning, J. J., and R. E. Mebius. 2012. Interdependence of stromal and immune cells for lymph node function. *Trends Immunol.* 33: 264–270.
7. Khan, I. S., M. L. Mouchess, M. L. Zhu, B. Conley, K. J. Fasano, Y. Hou, L. Fong, M. A. Su, and M. S. Anderson. 2014. Enhancement of an anti-tumor immune response by transient blockade of central T cell tolerance. *J. Exp. Med.* 211: 761–768.
8. Lo Iacono, N., H. C. Blair, P. L. Poliani, V. Marrella, F. Ficara, B. Cassani, F. Facchetti, E. Fontana, M. M. Guerrini, E. Traggiai, et al. 2012. Osteopetrosis rescue upon RANKL administration to Rankl(−/−) mice: a new therapy for human RANKL-dependent ARO. *J. Bone Miner. Res.* 27: 2501–2510.
9. Hanada, R., T. Hanada, V. Sigl, D. Schramek, and J. M. Penninger. 2011. RANKL/RANK-beyond bones. *J. Mol. Med.* 89: 647–656.
10. Lo Iacono, N., A. Pangrazio, M. Abinun, R. Bredius, M. Zecca, H. C. Blair, P. Vezzoni, A. Villa, and C. Sobacchi. 2013. RANKL cytokine: from pioneer of the osteoimmunology era to cure for a rare disease. *Clin. Dev. Immunol.* 2013: 412768.
11. Takayanagi, H. 2012. New developments in osteoimmunology. *Nat. Rev. Rheumatol.* 8: 684–689.
12. Manilay, J. O., and M. Zouali. 2014. Tight relationships between B lymphocytes and the skeletal system. *Trends Mol. Med.* 20: 405–412.
13. Kim, D., R. E. Mebius, J. D. MacMicking, S. Jung, T. Cupedo, Y. Castellanos, J. Rho, B. R. Wong, R. Josien, N. Kim, et al. 2000. Regulation of peripheral lymph node genesis by the tumor necrosis factor family member TRANCE. *J. Exp. Med.* 192: 1467–1478.
14. Onal, M., J. Xiong, X. Chen, J. D. Thostenson, M. Almeida, S. C. Manolagas, and C. A. O'Brien. 2012. Receptor activator of nuclear factor κB ligand (RANKL) protein expression by B lymphocytes contributes to ovariectomy-induced bone loss. *J. Biol. Chem.* 287: 29851–29860.
15. Perlot, T., and J. M. Penninger. 2012. Development and function of murine B cells lacking RANK. *J. Immunol.* 188: 1201–1205.
16. Yeo, L., H. Lom, M. Juarez, M. Snow, C. D. Buckley, A. Filer, K. Raza, and D. Scheel-Toellner. 2014. Expression of FcRL4 defines a pro-inflammatory, RANKL-producing B cell subset in rheumatoid arthritis. *Ann. Rheum. Dis.* DOI: 10.1136/annrheumdis-2013-204116.
17. Yeo, L., K. M. Toellner, M. Salmon, A. Filer, C. D. Buckley, K. Raza, and D. Scheel-Toellner. 2011. Cytokine mRNA profiling identifies B cells as a major source of RANKL in rheumatoid arthritis. *Ann. Rheum. Dis.* 70: 2022–2028.
18. Guerrini, M. M., C. Sobacchi, B. Cassani, M. Abinun, S. S. Kilic, A. Pangrazio, D. Moratto, E. Mazzolari, J. Clayton-Smith, P. Orchard, et al. 2008. Human osteoclast-poor osteopetrosis with hypogammaglobulinemia due to TNFRSF11A (RANK) mutations. *Am. J. Hum. Genet.* 83: 64–76.
19. Sobacchi, C., A. Frattini, M. M. Guerrini, M. Abinun, A. Pangrazio, L. Susani, R. Bredius, G. Mancini, A. Cant, N. Bishop, et al. 2007. Osteoclast-poor human osteopetrosis due to mutations in the gene encoding RANKL. *Nat. Genet.* 39: 960–962.
20. Karlsson, M. C., R. Guinamard, S. Bolland, M. Sankala, R. M. Steinman, and J. V. Ravetch. 2003. Macrophages control the retention and trafficking of B lymphocytes in the splenic marginal zone. *J. Exp. Med.* 198: 333–340.
21. Pereira, J. P., L. M. Kelly, and J. G. Cyster. 2010. Finding the right niche: B-cell migration in the early phases of T-dependent antibody responses. *Int. Immunol.* 22: 413–419.
22. Cerutti, A., M. Cols, and I. Puga. 2013. Marginal zone B cells: virtues of innate-like antibody-producing lymphocytes. *Nat. Rev. Immunol.* 13: 118–132.
23. Wardemann, H., T. Boehm, N. Dear, and R. Carsetti. 2002. B-1a B cells that link the innate and adaptive immune responses are lacking in the absence of the spleen. *J. Exp. Med.* 195: 771–780.
24. Martin, F., A. M. Oliver, and J. F. Kearney. 2001. Marginal zone and B1 B cells unite in the early response against T-independent blood-borne particulate antigens. *Immunity* 14: 617–629.
25. Oracki, S. A., J. A. Walker, M. L. Hibbs, L. M. Corcoran, and D. M. Tarlinton. 2010. Plasma cell development and survival. *Immunol. Rev.* 237: 140–159.
26. Ramiscal, R. R., and C. G. Vinuesa. 2013. T-cell subsets in the germinal center. *Immunol. Rev.* 252: 146–155.
27. Viau, M., and M. Zouali. 2005. B-lymphocytes, innate immunity, and autoimmunity. *Clin. Immunol.* 114: 17–26.
28. Hoyer, B. F., K. Moser, A. E. Hauser, A. Peddinghaus, C. Voigt, D. Eilat, A. Radbruch, F. Hiepe, and R. A. Manz. 2004. Short-lived plasmablasts and long-lived plasma cells contribute to chronic humoral autoimmunity in NZB/W mice. *J. Exp. Med.* 199: 1577–1584.
29. Luzina, I. G., S. P. Atamas, C. E. Storrer, L. C. daSilva, G. Kelsoe, J. C. Papadimitriou, and B. S. Handwerger. 2001. Spontaneous formation of germinal centers in autoimmune mice. *J. Leukoc. Biol.* 70: 578–584.
30. Li, Y., G. Toraldo, A. Li, X. Yang, H. Zhang, W. P. Qian, and M. N. Weitzmann. 2007. B cells and T cells are critical for the preservation of bone homeostasis and attainment of peak bone mass in vivo. *Blood* 109: 3839–3848.
31. Yoshizaki, A., T. Miyagaki, D. J. DiLillo, T. Matsushita, M. Horikawa, E. I. Kountikov, R. Spolski, J. C. Poe, W. J. Leonard, and T. F. Tedder. 2012. Regulatory B cells control T-cell autoimmunity through IL-21-dependent cognate interactions. *Nature* 491: 264–268.

32. DiLillo, D. J., T. Matsushita, and T. F. Tedder. 2010. B10 cells and regulatory B cells balance immune responses during inflammation, autoimmunity, and cancer. *Ann. N. Y. Acad. Sci.* 1183: 38–57.
33. Fillatreau, S. 2013. Cytokine-producing B cells as regulators of pathogenic and protective immune responses. *Ann. Rheum. Dis.* 72(Suppl. 2): ii80–ii84.
34. Mauri, C., and A. Bosma. 2012. Immune regulatory function of B cells. *Annu. Rev. Immunol.* 30: 221–241.
35. Takayanagi, H. 2007. Osteoimmunology: shared mechanisms and crosstalk between the immune and bone systems. *Nat. Rev. Immunol.* 7: 292–304.
36. Horowitz, M. C., J. A. Fretz, and J. A. Lorenzo. 2010. How B cells influence bone biology in health and disease. *Bone* 47: 472–479.
37. Kawabe, T., T. Naka, K. Yoshida, T. Tanaka, H. Fujiwara, S. Suematsu, N. Yoshida, T. Kishimoto, and H. Kikutani. 1994. The immune responses in CD40-deficient mice: impaired immunoglobulin class switching and germinal center formation. *Immunity* 1: 167–178.
38. Bolduc, A., E. Long, D. Stapler, M. Cascalho, T. Tsubata, P. A. Koni, and M. Shimoda. 2010. Constitutive CD40L expression on B cells prematurely terminates germinal center response and leads to augmented plasma cell production in T cell areas. *J. Immunol.* 185: 220–230.
39. Erickson, L. D., B. G. Durell, L. A. Vogel, B. P. O'Connor, M. Cascalho, T. Yasui, H. Kikutani, and R. J. Noelle. 2002. Short-circuiting long-lived humoral immunity by the heightened engagement of CD40. *J. Clin. Invest.* 109: 613–620.
40. Kishi, Y., Y. Aiba, T. Higuchi, K. Furukawa, T. Tokuhisa, T. Takemori, and T. Tsubata. 2010. Augmented antibody response with premature germinal center regression in CD40L transgenic mice. *J. Immunol.* 185: 211–219.
41. Bachmann, M. F., B. R. Wong, R. Josien, R. M. Steinman, A. Oxenius, and Y. Choi. 1999. TRANCE, a tumor necrosis factor family member critical for CD40 ligand-independent T helper cell activation. *J. Exp. Med.* 189: 1025–1031.
42. Teitelbaum, S. L. 2000. Bone resorption by osteoclasts. *Science* 289: 1504–1508.
43. Yun, T. J., M. D. Tallquist, A. Aicher, K. L. Rafferty, A. J. Marshall, J. J. Moon, M. E. Ewings, M. Mohaupt, S. W. Herring, and E. A. Clark. 2001. Osteoprotegerin, a crucial regulator of bone metabolism, also regulates B cell development and function. *J. Immunol.* 166: 1482–1491.
44. Sabat, R. 2010. IL-10 family of cytokines. *Cytokine Growth Factor Rev.* 21: 315–324.
45. Saraiva, M., and A. O'Garra. 2010. The regulation of IL-10 production by immune cells. *Nat. Rev. Immunol.* 10: 170–181.
46. Mauri, C., and P. A. Blair. 2010. Regulatory B cells in autoimmunity: developments and controversies. *Nat. Rev. Rheumatol.* 6: 636–643.
47. Blair, P. A., K. A. Chavez-Rueda, J. G. Evans, M. J. Shlomchik, A. Eddaoudi, D. A. Isenberg, M. R. Ehrenstein, and C. Mauri. 2009. Selective targeting of B cells with agonistic anti-CD40 is an efficacious strategy for the generation of induced regulatory T2-like B cells and for the suppression of lupus in MRL/lpr mice. *J. Immunol.* 182: 3492–3502.
48. Ries, S., E. Hilgenberg, V. Lampropoulou, P. Shen, V. D. Dang, S. Wilantri, I. Sakwa, and S. Fillatreau. 2014. B-type suppression: a role played by "regulatory B cells" or "regulatory plasma cells"? *Eur. J. Immunol.* 44: 1251–1257.
49. Koni, P. A., A. Bolduc, M. Takezaki, Y. Ametani, L. Huang, J. R. Lee, S. L. Nutt, M. Kamanaka, R. A. Flavell, A. L. Mellor, et al. 2013. Constitutively CD40-activated B cells regulate CD8 T cell inflammatory response by IL-10 induction. *J. Immunol.* 190: 3189–3196.
50. Matsumoto, M., A. Baba, T. Yokota, H. Nishikawa, Y. Ohkawa, H. Kayama, A. Kallies, S. L. Nutt, S. Sakaguchi, K. Takeda, et al. 2014. Interleukin-10-producing plasmablasts exert regulatory function in autoimmune inflammation. *Immunity* 41: 1040–1051.
51. Hikosaka, Y., T. Nitta, I. Ohigashi, K. Yano, N. Ishimaru, Y. Hayashi, M. Matsumoto, K. Matsuo, J. M. Penninger, H. Takayanagi, et al. 2008. The cytokine RANKL produced by positively selected thymocytes fosters medullary thymic epithelial cells that express autoimmune regulator. *Immunity* 29: 438–450.
52. Breitfeld, D., L. Ohl, E. Kremmer, J. Ellwart, F. Sallusto, M. Lipp, and R. Förster. 2000. Follicular B helper T cells express CXC chemokine receptor 5, localize to B cell follicles, and support immunoglobulin production. *J. Exp. Med.* 192: 1545–1552.
53. Defrance, T., B. Vanbervliet, F. Brière, I. Durand, F. Rousset, and J. Banchereau. 1992. Interleukin 10 and transforming growth factor beta cooperate to induce anti-CD40-activated naive human B cells to secrete immunoglobulin A. *J. Exp. Med.* 175: 671–682.
54. Rousset, F., D. Vautrin, and M. Solignac. 1992. Molecular identification of Wolbachia, the agent of cytoplasmic incompatibility in Drosophila simulans, and variability in relation with host mitochondrial types. *Proc. Biol. Sci.* 247: 163–168.
55. Heine, G., G. Drozdenko, J. R. Grün, H. D. Chang, A. Radbruch, and M. Worm. 2014. Autocrine IL-10 promotes human B-cell differentiation into IgM- or IgG-secreting plasmablasts. *Eur. J. Immunol.* 44: 1615–1621.
56. Boumans, M. J., R. M. Thurlings, L. Yeo, D. Scheel-Toellner, K. Vos, D. M. Gerlag, and P. P. Tak. 2012. Rituximab abrogates joint destruction in rheumatoid arthritis by inhibiting osteoclastogenesis. *Ann. Rheum. Dis.* 71: 108–113.
57. Dimitroulas, T., S. N. Nikas, P. Trontzas, and G. D. Kitas. 2013. Biologic therapies and systemic bone loss in rheumatoid arthritis. *Autoimmun. Rev.* 12: 958–966.